AIMS Materials Science, 4(3): 706-737.
DOI: 10.3934/matersci.2017.3.706
Received: 06 March 2017
Accepted: 01 June 2017
Published: 13 June 2017

http://www.aimspress.com/journal/Materials

Review

Developments in the evaluation of elastic properties of carbon nanotubes and their heterojunctions by numerical simulation

Nataliya A. Sakharova [1,*], Jorge M. Antunes [1,2], Andre F. G. Pereira [1], and Jose V. Fernandes [1]

[1] CEMMPRE—Department of Mechanical Engineering, University of Coimbra, Rua Luís Reis Santos, Pinhal de Marrocos, 3030-788 Coimbra, Portugal
[2] Escola Superior de Tecnologia de Abrantes, Instituto Politécnico de Tomar, Rua 17 de Agosto de 1808-2200 Abrantes, Portugal

* **Correspondence:** Email: nataliya.sakharova@dem.uc.pt; Tel: +351-239-790-747.

Abstract: High-tech miniaturization is a strategic area to empower new scientific challenges for which carbon nanotubes are ideal candidates with outstanding electronic, optical and mechanical properties. Carbon nanotubes and their heterojunctions are efficient components for reinforcement of composites, for constructing micro- and nanodevices, and for designing new materials with required electronic and mechanical properties. The carbon nanotubes have been studied experimentally, but a big inconsistency in experimental results has been observed, because of the technical difficulties to operate with nanoscale objects. For this reason, modelling and computer simulation for predicting their mechanical properties have received much attention. This review attempts to classify the accomplishments in predicting of the elastic properties of carbon nanotubes and their heterojunctions by analytical and computational approaches. The literature results concerning Young's modulus, shear modulus and Poisson's ratio of perfect and with defects single-walled and multi-walled carbon nanotubes and their heterojunction are analysed and systematized.

Keywords: carbon nanotubes; heterojunctions; elastic properties; numerical simulation

1. Introduction

For more than two decades, systematic research has been conducted for developing nano-materials such as carbon nanotubes (CNTs) that are unique nanostructures with regard to their mechanical, optical, thermal and electrical properties [1], the latter of which can also be seen as a

prototypical quantum nanowire, where quantum effects influence the electrical transport properties [2]. Carbon nanotubes are optimal structures to reinforce composites, building blocks for optical and electronic nanodevices [3,4,5], and efficient components for designing new materials with required electronic and mechanical properties [6]. From the point of view of construction of nanodevices, the CNT heterojunctions are necessary constituents for the circuits, amplifiers, switches and nanodiodes [7]. In order to design composites reinforced with CNTs, nanosensors and CNT-based electronic devices, the understanding of the CNTs' mechanical properties is indispensable, since the stability and efficiency of nanodevices are highly dependent on the mechanical properties of their components.

There are two approaches commonly used to assess the elastic properties of CNTs: experimental and computational. Experimental methods for measuring the elastic modulus of CNTs, based on *in situ* techniques of atomic force microscopy (AFM) and transmission electron microscopy (TEM) have been established [8–11]. All experimental studies show the unparalleled mechanical properties of CNTs. However, there is inconsistency in the experimental mechanical results reported in the literature, owing to the complexity of the characterization of nanomaterials at the atomic scale. In fact, the experimental studies still show a wide scattering of their results. The reason of the scattering can also be associated with defects in the CNT's structure: it is almost impossible to produce carbon nanotubes with a perfect structure because of the manufacturing constraints. It should be noted, that the lack of perfection of the lattice of the CNTs, used in experimental studies, can influence the results [12,13]. Due to these reasons, modelling and computer simulation for predicting the mechanical properties of CNTs have been developed.

A considerable part of the theoretical investigations has been devoted to the modelling and the evaluation of the elastic properties, mainly Young's modulus, of perfect (without defects) single-walled carbon nanotubes (SWCNTs), as for example [14,15,16]. Less attention has been paid to understanding the mechanical behaviour of SWCNT with defects and nanotube heterojunctions. The building of adequate numerical models of the multi-walled carbon nanotubes (MWCNTs) has also received less analysis so far, in spite of their high level of commercialization.

Two recent review articles have been published under the scope of the work on carbon nanotubes. One, conducted by Rafiee and Moghadam [17], concerns the modelling techniques and simulation of mechanical and thermal properties, buckling and vibrational behaviour of perfect SWCNTs. Moreover, Yengejeh et al. [18] have reviewed the advances in the modelling and numerical characterization of the mechanical properties, buckling and vibrational behaviour of imperfect (with defects) and structurally modified carbon nanotubes, including CNT heterojunctions.

The present work is focused on the achievements in the characterisation of mechanical properties of perfect and imperfect (with defects) single-walled and multi-walled CNTs, as well as CNT heterojunctions (HJs) by modelling their structure and mechanical behaviour, using theoretical (analytical and numerical) approaches.

Following this introduction, the review gives a brief introduction to the atomic structure of CNTs and their heterojunctions. Afterwards, the modelling techniques for characterization of the CNTs' mechanical behaviour are described and the outcomes attained in the evaluation of the elastic properties (Young's and shear moduli, Poisson's ratio) of SWCNTs, MWCNTs and CNT heterojunctions, with and without vacancy defects, are presented and discussed.

2. Atomic Structure of CNTs and Their Heterojunctions

A simple way to describe an ideal single-walled nanotube is as a rolled-up graphene sheet giving rise to a hollow cylinder, whose surface is composed of hexagonal carbon rings (see, for example [19,20]). The hexagonal pattern is repeated periodically, leading to binding of each carbon atom to three neighbouring atoms by covalent bonds. A schematic illustration of an unrolled hexagonal graphene sheet is shown in Figure 1. The symmetry of the atomic structure of a nanotube is characterized by the chirality, which is defined by the chiral vector $\boldsymbol{C_h}$:

$$\boldsymbol{C_h} = n\boldsymbol{a_1} + m\boldsymbol{a_2} \tag{1}$$

where n and m are integers, and $\boldsymbol{a_1}$ and $\boldsymbol{a_2}$ are the unit vectors of the hexagonal lattice.

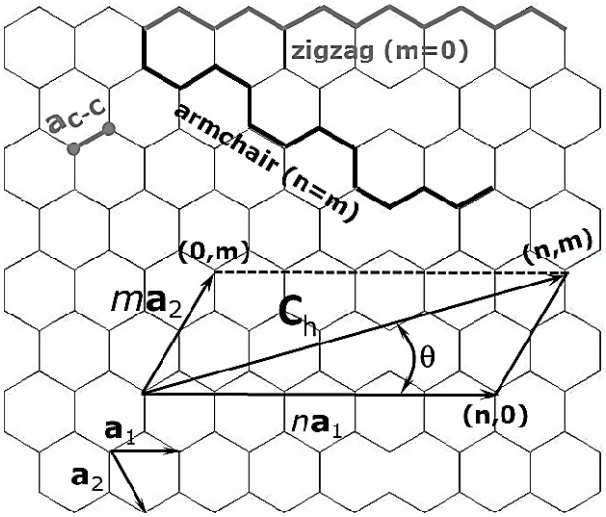

Figure 1. Illustration of an unrolled graphene sheet with definition of the chiral vector.

The length of the unit vector $\boldsymbol{a}$ is defined as $a = \sqrt{3}a_{C-C}$ with the equilibrium carbon–carbon (C–C) covalent bond length a_{C-C} usually taken to be 0.1421 nm [2]. The nanotube circumference, L_c, and diameter, D_n are:

$$L_c = |\boldsymbol{C_h}| = a\sqrt{n^2 + nm + m^2} \tag{2}$$

$$D_n = \frac{L_c}{\pi} \tag{3}$$

The chiral angle, θ, is defined by the angle between the chiral vector $\boldsymbol{C_h}$ and the direction (*n*, *0*). The chiral angle, θ, is given by Dresselhaus et al. [19]:

$$\theta = \sin^{-1}\frac{\sqrt{3}m}{2\sqrt{n^2 + nm + m^2}} \tag{4}$$

Three main symmetry groups of single-walled carbon nanotubes (SWCNTs) exist. When $n = m$, the structure *(n, n)* is called armchair configuration; when $m = 0$, the structure *(n, 0)* is named zigzag; when $n \neq m$, the structure *(n, m)* is chiral. These three major categories of carbon

nanotubes can also be defined based on the chiral angle θ, as can be deduced from Eq. (4). For the two limiting chiral angles of 0° and 30°, the nanotubes are referred to as non-chiral, zigzag and armchair, respectively. For θ different from 0° and 30°, the nanotubes are designated as chiral. Schematic representations of three types of SWCNTs are shown on the Figure 2.

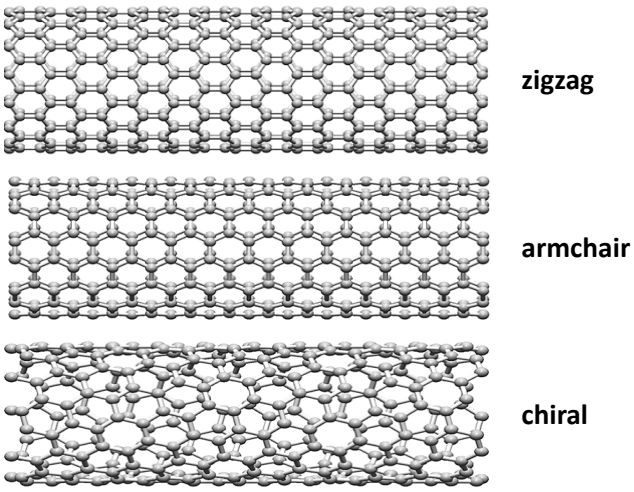

Figure 2. Three structural models of SWCNTs. Obtained by using Nanotube Modeler © software.

The multi-walled carbon nanotubes are composed of multiple coaxial SWCNTs, which interact with each other by non-covalent interactions, the weak van der Waals forces which can be adequately modelled by using the Lennard–Jones potential.

The CNT heterojunction can be represented as two CNTs that are connected by introducing an intermediate region with Stone–Wales defects [21], as illustrated in Figure 3 (Figure 3(a): heptagon defect; Figure 3(b): pentagon defect). Similarly to SWCNT structures, the geometrical parameters of heterojunctions (HJs) are the chirality, and diameter. There are two main heterojunction configurations [21]: (i) cone-heterojunctions (HJs of nanotubes with a given chiral angle but different radii) as armchair–armchair and zigzag–zigzag HJs, and (ii) radius-preserving heterojunctions (HJs preserving the radii, but with different chiral angles of the constituent nanotubes) as armchair–zigzag or chiral–armchair (or zigzag) HJs. Ghavamian et al. [22] also define heterojunctions of armchair–zigzag or chiral–armchair (or zigzag), with different radii, that designate as HJ with bent connection, in contrast to the cone-heterojunctions that they name as HJ with straight connection. According to the study of Yao et al. [23] most HJs (>95%) are cone-heterojunctions type. The geometry of different type of heterojunctions is shown in Figure 4(a–c).

The overall length of the heterojunction is defined as follows:

$$L_{HJ} = L_1 + L_2 + L_3 \tag{5}$$

where L_1, L_2 are the lengths of the narrower and wider SWCNTs regions, respectively, and L_3 is the length of the connecting region (see, Figure 4(a)).

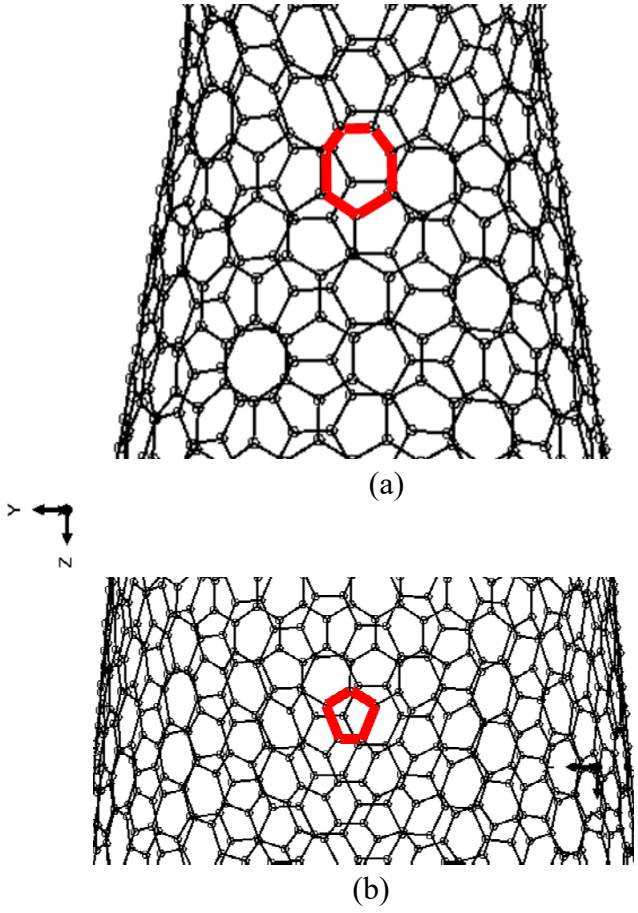

Figure 3. Defects (in bold red) in the connecting region of the armchair–armchair (10, 10)–(20, 20) heterojunction: (a) Heptagon defect; (b) Pentagon defect. HJ is obtained by using academic software CoNTub 1.0 © [21].

When the heterojunction consists of two SWCNTs with different diameters (i.e., cone-heterojunction), the diameter of HJ can be characterised by the average of the narrower and wider diameters (see, for example [21]):

$$\overline{D}_{HJ} = \frac{1}{2}(D_{n1} + D_{n2}) \tag{6}$$

And the aspect ratio of the cone-heterojunction is defined as [24]:

$$\eta = \frac{L_3}{\overline{D}_{HJ}} \tag{7}$$

According to Sakharova et al. [25], the length of the connecting region, L_3, follows a quasi linear function with $(D_{n2} - D_{n1})$, for armchair–armchair and zigzag–zigzag cone-heterojunctions. The fitted straight line equation allows determining L_3 as follows:

$$L_3 = 2.9157(D_{n2} - D_{n1}) \tag{8}$$

where D_{n1} and D_{n2} are diameters of the narrow and wider nanotubes, respectively. Similar relationship for the connecting region of cone-heterojunctions was proposed by Qin et al. [26],

basing on geometrical analysis:

$$L_3 = \frac{\sqrt{3}}{2}\pi(D_{n2} - D_{n1}) = 2.7207(D_{n2} - D_{n1}) \quad (9)$$

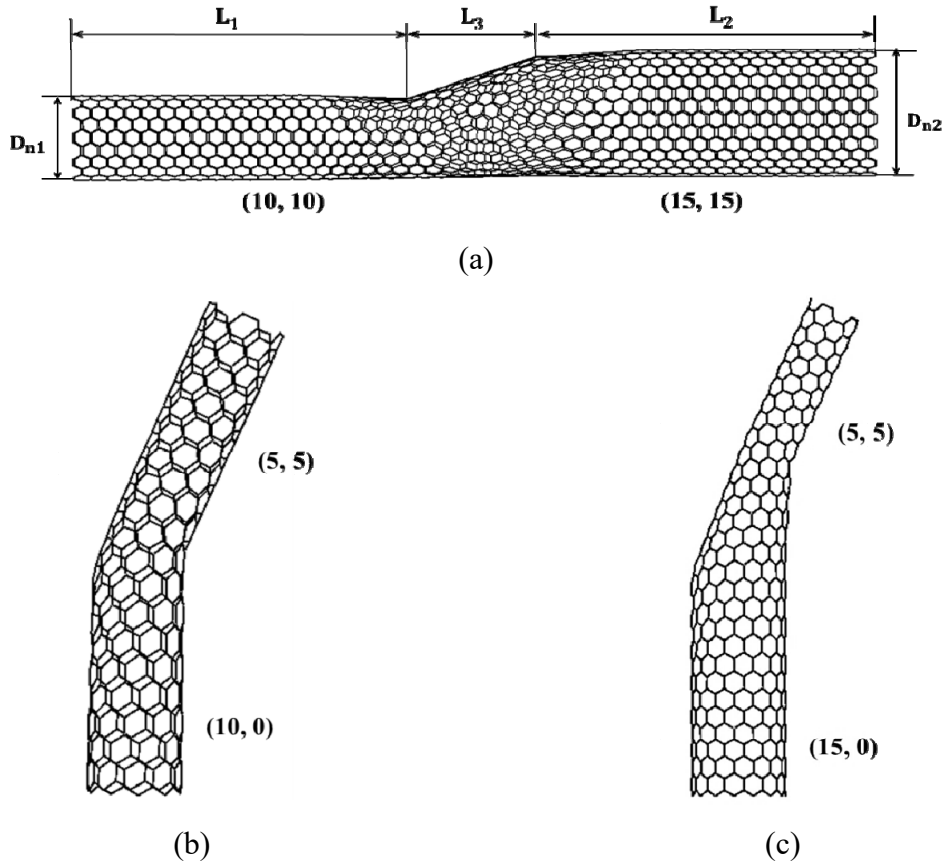

Figure 4. Geometry of (a) cone armchair–armchair (10, 10)–(15, 15) HJ; (b) radius-preserving armchair–zigzag (5, 5)–(10, 0) HJ and (c) armchair–zigzag (5, 5)–(15, 0) HJ with bent connection. HJs structures obtained by using academic software CoNTub 1.0 © [21].

3. Modelling Techniques

The theoretical approaches for the modelling and characterization of the CNTs' mechanical behaviour can be grouped into three main categories: the atomistic approach, the continuum mechanics (CM) approach and the nanoscale continuum modelling (NCM) approach, also called molecular structural mechanics (MSM), as it was firstly introduced by Rafie and Moghadam [17], who discussed the applicability and efficiency of these three approaches toward understanding behaviour of carbon nanotubes.

During the first years of theoretical studies on CNTs, solely atomistic modelling, which calculates the positions of atoms based on their interactive forces and boundary conditions (see, for example, [27]), has been used. Atomistic modelling, used solely during the first years of theoretical studies on CNTs. Atomistic modelling comprises the molecular dynamics (MD) [28–34] and *ab initio* approach [35]. MD is a numerical technique simulating the motions of a system of particles

based on Newton's second law. The key to the MD simulation is to choose an appropriate potential energy model to describe the bonding and nonbonding interactions between carbon atoms in nanotube. These interactions are described by means of analytical or empirical potential functions. Lu [29] employed an empirical force-constant model, where the atomic interactions near the equilibrium structure were approximated by the sum of pairwise harmonic potentials between atoms. Jin and Yuan [30] in their MD simulation adopted force-constant approach, using force potentials to describe the interatomic atomic interactions. In the MD simulation studies of Liew et al. [31] and WenXing et al. [32], the interaction force between atoms was modelled using a second generation reactive empirical bond order (REBO) potential coupled with the Lennard–Jones potential. Yakobson et al. [28] used a many-body interatomic potential (Tersoff–Brenner potential) with a continuum shell model. Zhang et al., [33] compared two MD modelling approaches, using for this purpose the Tersoff–Brenner and modified Morse potentials. The approach of Cheng et al. [34] integrated classical MD simulation with Tersoff–Brenner potential and nanoscale continuum modelling. Wilmes and Pinho [36] proposed a new molecular dynamics finite element method (MDFEM), where the equilibrium equations of MD are embedded within computationally more favourable FE method. Also, tight-binding molecular dynamics (TBMD), another atomistic modelling method, which offers a compromise between *ab initio* methods and MD simulations with empirical potentials, was developed [37,38]. Molecular dynamics can be used in large systems and provide good predictions of CNTs' mechanical properties under different loading conditions, but it is still restricted owing to its being very time consuming, especially when long or multi-walled CNTs are simulated. Generally, *ab initio* methods give more accurate results than MD, but they are highly expensive in terms of computational resources and are limited to be used for a small number of molecules or atoms. In recent years, the atomistic approaches, due to their big computation cost, have been gradually replaced by continuum approaches, which are at the moment the most indicated for effective computational simulation of large systems.

The basic assumption of the continuum mechanics (CM) approach consists of the modelling of CNTs as a continuum structure, concerning the distribution of mass, stiffness, etc., i.e., the real discrete structure of the nanotubes is neglected and replaced by a continuum medium. Some authors have explored continuum shell modelling for studying the mechanical behaviour of CNTs [39–42]. However, the chirality of CNTs is not taken into account in the continuous shell approach, and so its effect on the mechanical behaviour of CNTs cannot be captured. To overcome this obstacle, Chang proposed an anisotropic shell model for SWCNTs [43] that can predict some anisotropic effects, related to chirality. Besides shell structures, other continuum structures, such as tubes and plates, are employed in CM approaches. In the models of Sears and Batra [44], and Gupta and Batra [45] the whole single-walled CNT's structure was simulated as an equivalent continuum tube. Wang [46] employed the equivalent elastic plate model. Arash and Wang [47] show the advantages of the continuum theory applied to the modelling of shells and plates. However, whatever the type of the CM approach, the replacement of the whole CNT's structure by a continuum element is not a completely satisfactory method to evaluate CNT's mechanical properties, because it depends on additionally introduced material properties and it is restricted to certain mechanical behaviours of CNTs [17].

The nanoscale continuum modelling (or molecular structure mechanics: NCM/MSM) approach consists of replacing the carbon–carbon (C–C) bond with a continuum element. As a result, continuum mechanics theories can be used at the nanoscale, i.e., the connection between molecular

configuration and solid mechanics is considered. The NCM/MSM approach consists of considering different elements, such as rod, truss, spring and beam, well described in elasticity theory, to simulate C–C bonds (see, for example, [14,16,48–52]). The first nanoscale continuum model of CNTs was developed by Odegard et al. [48] and consisted of a continuum truss model. The disadvantage of the truss model is the impossibility of describing the CNTs' mechanical behaviour under torsional load, because the out-of-plane torsion of the C–C bond cannot be taken into account. Various FE models where the C–C bonds are simulated using diverse kinds of elastic spring elements, such as linear, non-linear, rotational, torsional, have been recently reported [15,53–59]. Although the use of spring elements is an effective way for simulating the bond angle variations, the accuracy of the determination of the elastic properties depends on the choice of the potential function for the calculation of the force constants.

Since Li and Chou [49] established a direct relationship between the structural mechanics parameters of the beam element and the molecular mechanics parameters, the NCM approach, employing the beam element for replacing the C–C bond, has been successfully used to simulate the mechanical behaviour of CNT, although with different formulations of the inter-atomic molecular potential energies and boundary conditions [14,16,51,52,60–67]. The FE models, which employed beam elements, developed by Tserpes and Papanikos [14], To [60], Papanikos et al. [61], Ávila and Lacerda [62], Sakharova et al. [16], and Ghadyani and Öchsner [67] differ from each other mainly due to the boundary conditions and the method for the Young's modulus calculation. The recent three-dimensional (3D) FE model of Lu and Hu [65] used the same formulation for the potential energy of the covalent system, but considering an elliptical cross-section area of the equivalent beam. In the works of Chen et al. [51] and Eberhardt and Wallmersperger [52] the original Li and Chou [46] model was modified, mainly with respect to the bending rigidity of the beam element. For this purpose, rectangular beam elements with minor and major axes of bending rigidities were considered by Chen et al. [51], for representation of the covalent bonds. Eberhardt and Wallmersperger [52] proposed that the geometrical and material parameters defining the beams can be obtained with the help of a specific modified molecular structural mechanics approach which is consistent in terms of the involved energies. In another analytical approach developed by Shokrieh and Rafiee [63], the deformations of the beam elements were obtained using the Castiglinao's theorem. In the works of Her and Liu [64], and Mohammadpour and Awang [61] the modified Morse potential function for the potential energy of the covalent system was applied for describing the non-linear behaviour of C–C bonds. In their recent work, Giannopoulos et al. [68], who employed linear bar elements to simulate interatomic interactions between carbon atoms, showed the efficiency of this model for the investigation of the stability of CNTs under compressive and radial loads. In contrast to abovementioned works, which used classical truss, spring, bar and beam elements to simulate C–C bond, Nasdala and Ernst [69] developed a special 4-node element for computing internal forces of the molecular system without necessity of the determination of material parameters. In a recent review, Rafiee and Moghadam [17] concluded that NCM is an efficient modelling approach for simulation of the CNT's behaviour, which does not require intensive computation and can be applied to complex systems without limitation of length scales, when comparing with atomistic modelling.

The knowledge of the bond length of CNTs is of fundamental importance for the modelling of their mechanical properties. Its value is generally considered to be equal to that of the graphene sheet, a_{C-C} = 0.1421 nm. Nevertheless other values have been considered: for example, Budyka [70] reported that rolling up the graphene sheet into armchair SWCNT leads to a slight elongation of the

C–C bond. The value of the wall thickness of CNTs is varied in the literature sources. Although a few theoretical reports have provided values for nanotube wall thickness, t_n, that range from 0.064 [40] to 0.69 nm [48], the most widely used value is 0.34 nm (equal to the interlayer spacing of graphite). Most of the elastic properties results, obtained in the theoretical and numerical simulation studies, depend on the assumption of the value of CNT's wall thickness. In recent times, an attempt to acquire a thickness free expression for the CNT's stiffness has been undertaken by Ghadyani and Öchsner [71].

4. Elastic Properties of the Single-walled Carbon Nanotubes

4.1. Rigidities of SWCNTs

Numerical simulation studies related to nanotube rigidities are infrequent in the literature [16,61,72]. The linear relationships between the nanotube elastic rigidities and chiral indices, n, were firstly obtained by Papanikos et al. [61] for non-chiral SWCNTs. Later, in the works of Sakharova et al. [16] and Pereira et al. [72], single equations valid for armchair, zigzag and chiral SWCNTs, which allows correlating the tensile, EA, bending, EI, and torsional, GJ, rigidities of the SWCNT with the nanotube diameter, D_n, were proposed:

$$EA = \alpha(D_n - D_0) \tag{10}$$

$$EI = \beta(D_n - D_0)^3 \tag{11}$$

$$GJ = \gamma(D_n - D_0)^3 \tag{12}$$

The values of the fitting parameters α, β, γ and D_0 obtained in the works [16,72], and those calculated based on the results of the work [61] are summarized in Table 1.

Table 1. Fitting parameters α, β, γ and D_0.

Parameter	Value* [16,72]	Value** [61]
$\alpha, nN \cdot nm^{-1}$	1131.66	1128.15
$\beta, nN \cdot nm^{-1}$	143.48	142.54
$\gamma,\ nN \cdot nm^{-1}$	130.39	135.38
$D_0, nm/n_0$	3.5×10^{-3}	0

* Includes armchair, zigzag and three families, $\theta = 8.9°, 13.9°, 19.1°$, of chiral SWCNTs.

** Includes armchair and zigzag SWCNTs (these values were obtained by equations similar to (10–12), in which n and n_0 replace D_n and D_0, respectively).

The relationships (10–12) and the values of the parameters α, β, γ and D_0, in Table 1, allow easy evaluation of the Young's modulus and the shear modulus as a function of the nanotube diameter [16,72]:

$$E = \frac{\alpha(D_n - D_0)}{\pi t_n \sqrt{8\frac{\beta(D_n - D_0)^2}{\alpha} - t_n^2}} \tag{13}$$

$$G = \frac{\gamma(D_n - D_0)}{2\pi t_n \left(\frac{\beta}{\alpha}\right)\sqrt{8\frac{\beta(D_n - D_0)^2}{\alpha} - t_n^2}} \tag{14}$$

4.2. Young's Modulus of SWCNTs

The results available in the literature, concerning the evaluation of SWCNTs' Young's modulus by different modelling methods, are summarized in Table 2. This table also includes experimental results reported by Krishnan et al. [73], who used thermal vibrations to estimate the Young's modulus, and the results of Yu et al. [74], who used the tensile test. The discrepancies observed between the Young's modulus results are due to different assumptions for the value of the CNT's wall thickness, t_n, (indicated in the Table 2), modelling approaches (MD, CM, NCM/MSM), potential functions, force fields constants, formulations for Young's modulus determinations, etc.

Reviewing the data available in the literature, concerning the prediction of the SWCNTs' elastic moduli, it can be seen that there are some discrepancies not only in the Young's modulus values, but also in the trend of their evolution with the nanotube diameter. This evolution can be separated into two tendencies, as shown in Figure 5: (i) the Young's modulus decreases with increase of the nanotube diameter, and with further increase of the nanotube diameter, the Young's modulus tends towards approximately a constant value [16,33,58,61,75] as shown in Figure 5(a); (ii) the Young's modulus is almost constant over the whole range of nanotube diameters [15,30,32,51,52,62,65,67,68] as shown in Figure 5(b). In some cases the Young's modulus slightly changes for small nanotube diameters [15,51,52,62,65,68]—see Figure 5(b). Concerning the effect of SWCNT's chirality on the Young's modulus, some authors reported similar values for non-chiral and chiral SWCNTs [16,61,75]. A small difference between the Young's modulus for armchair and zigzag SWCNTs is reported by Zhang et al. [31], Chen et al. [51] and Eberhardt and Wallmersperger [52], and for the three SWCNTs' chirality configurations by WengXing et al. [32], Avila and Lacerda [62], Lu and Hu [65], Ghadyani and Öchsner [67] and Giannopoulos et al. [68].

The evolution of the Young's modulus with the wall thickness follows a quasi-linear trend with the inverse of the wall thickness, $1/t_n$ as it was reported by Tserpes and Papanikos [14] and Avila and Lacerda [62], for the case of (8, 8) armchair SWCNT with diameter $D_n = 1.085\,nm$, by Ghadyani and Öchsner [71] for the (10, 10) armchair SWCNT with diameter $D_n = 1.356\,nm$, and by Sakharova et al. [16] for nanotubes with diameter $D_n \gtrsim 1.085\,nm$. In the latter case, for small nanotube diameters, $D_n \lesssim 1.085\,nm$, the deviation from the quasi-linear trend is pronounced for smaller values of $1/t_n$, particularly when the nanotube wall thickness approximates to half of its diameter, $t_n \gtrsim 1/2\,D_n$.

Table 2. Young's modulus results of SWCNTs, available in the literature.

	Reference		t_n, nm	Method	Young's modulus, E, TPa	
Atomistic modelling	[28]	Yakobson et al., 1996	0.066	MD: Tersoff–Brenner potential	5.5	average value
	[29]	Lu, 1997	0.34	MD: empirical force potential	0.97	average value
	[30]	Jin and Yuan, 2003	0.34	MD: force-constant approach	1.236	average value
	[31]	Liew et al., 2004	0.335	MD: REBO empirical potential	1.043	(10, 10) armchair
	[32]	WenXing et al., 2004	0.34	MD: REBO empirical potential	0.929	average value
	[33]	Zhang et al., 2005	0.335	MD: Tersoff–Brenner potential	1.08	converged value; zigzag
	[38]	Cheng et al., 2009	0.34	MD: Tersoff–Brenner potential	1.2	converged value; armchair
	[37]	Hernandez et al., 1998	0.34	TBMD	1.24	(10, 10) armchair
	[35]	Zhou et al., 2000	0.074	TBMD	5.1	average value
	[35]	Kudin et al., 2001	0.089	*ab initio*	3.859	average value
CM	[40]	Pantano et al., 2004	0.075	FE continuum shell model	4.84	average value
	[41]	Sears and Batra, 2004	0.134	Equivalent continuum tube	2.52	(16, 0) zigzag
	[44]	Kalamkarov et al., 2006	0.129	Analytical shell model	1.44	–
	[45]	Gupta and Batra, 2008	0.34	Equivalent continuum tube	0.964	av. value; non-chiral, chiral
NCM/MSM	[48]	Odegard et al., 2002	0.69	FE model: truss elements	0.49	–
	[53]	Natsuki et al., 2004	0.34	Analytical 2D model: springs	0.61	average value
	[54]	Meo and Rossi, 2006	0.34	FE model: non-linear springs and linear torsional springs	0.926	(10, 10) armchair
	[55]	Giannopoulos et al., 2008	0.34	3D FE model: linear springs	1.247	average value
	[58]	Parvaneh and Shariati, 2011	0.34	FE model: linear and non-linear springs	1.170	(22, 0) zigzag
	[15]	Rafiee and Heidarhaei, 2012	0.34	FE model: non-linear springs	1.325	converged value; non-chiral
	[59]	Mahmoudinezhad et al., 2012	0.34	3D FE model: rotational springs	0.85	converged value; armchair
	[49]	Li and Chou, 2003	0.34	3D FE model: linear beams	1.015	average value; non-chiral

NCM/MSM	[14]	Tserpes and Papanikos, 2005	0.147	3D FE model: linear beams	2.377	(8, 8) armchair
	[60]	To, 2006	0.34	3D FE model: linear beams	1.03	(17, 0) zigzag
	[61]	Papanikos et al., 2008	0.34	3D FE model: linear beams	1.072	converged value; non-chiral
	[62]	Ávila and Lacerda, 2008	0.34	3D FE model: linear beams	1.005	av. value; non-chiral, chiral
	[63]	Shokrieh and Rafiee, 2010	0.33	Analytical model: beams	1.042	converged value; armchair
	[51]	Cheng et al., 2010	–	Analytical model: rectangular beams	1.083	(24, 24) armchair
	[66]	Mohammadpour and Awang, 2011	0.147	FE model: nonlinear beams; Morse potential	2.037	(10, 10) armchair
	[64]	Her and Liu, 2012	0.34	FE model: nonlinear beams; Morse potential	0.927	(10, 10) armchair
	[65]	Lu and Hu, 2012	0.34	3D FE model: elliptical cross section beams	1.058	converged value; zigzag
	[68]	Giannopoulos et al., 2013	0.34	3D FE model: linear bar elements	1.347	converged value
	[67]	Ghadyani and Öchsner, 2015	0.34	3D FE model: linear beams	1.053	converged value; zigzag
	[52]	Eberhardt and Wallmersperger, 2015	0.34	3D FE model: tetrahedrons formed by beams	0.803	converged value; non-chiral
	[16]	Sakharova et al., 2015	0.34	3D FE model: linear beams	1.078	converged average value; non-chiral and chiral
Experimental	[73]	Krishnan et al., 1998	–	TEM, thermal vibrations	1.3 (−0.4/ +0.6)	average value; D_n in the range of $1.0 - 1.5\ nm$
	[74]	Yu et al., 2000	–	AFM, tensile test	1.0	average value

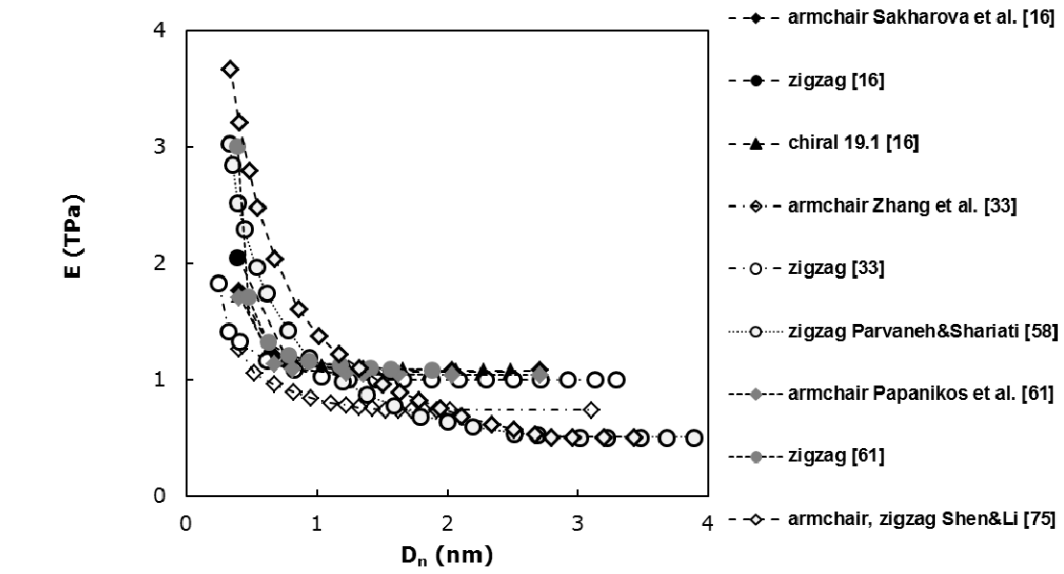

(a)

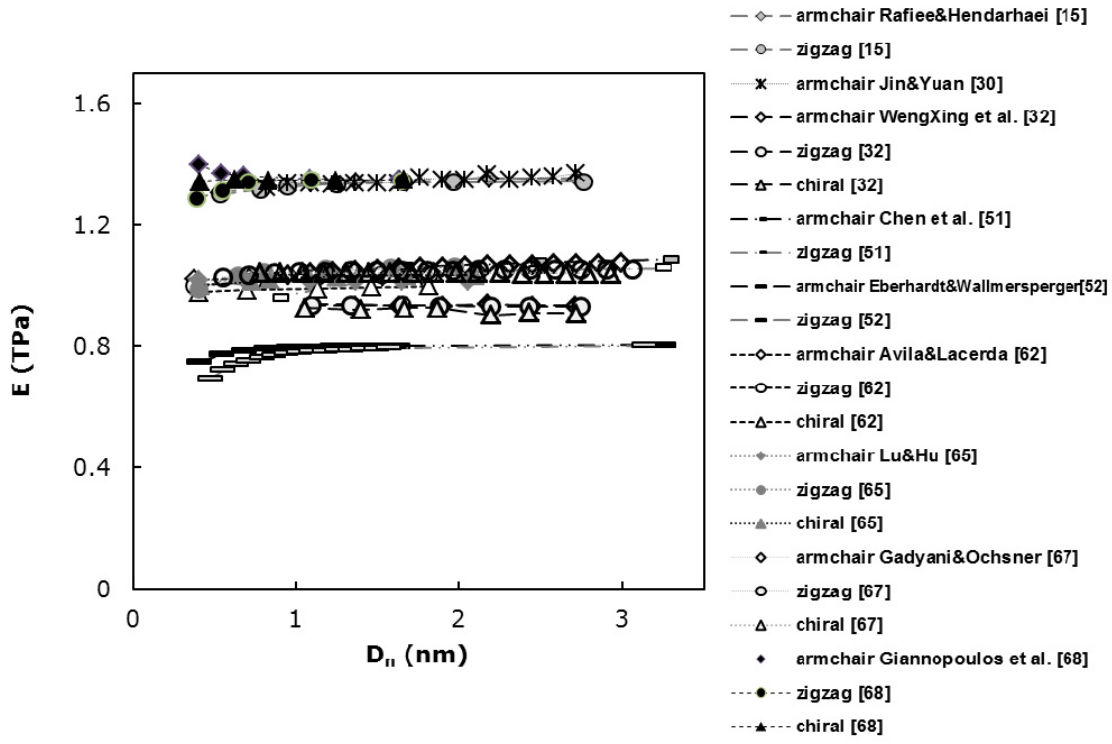

(b)

Figure 5. Literature results for the Young's modulus of SWCNTs. (a) and (b) show two different trends for the evolution of the Young's modulus E, with respect to the nanotube diameter, D_n.

4.3. Shear Modulus and Poisson's Ratio of SWCNTs

The works dealing with the evaluation of the shear modulus are scarcer than the ones determining the Young's modulus. It can be concluded from the available studies that there are two methods commonly used to evaluate the CNTs' shear modulus. One of them consists of the direct

determination of the shear modulus, from numerical simulation results of the torsion tests [30,45,50,55,60,61,65,68,76] or using analytical models that describe the torsional response [53,77,78]. The other method to assess the CNTs' shear modulus uses the results of the tensile test and resorts to the relationship between the Young's modulus and the Poisson's ratio, under isotropic conditions [30,50,75,79]. Only a few works compare results of the shear modulus, obtained by torsion and tensile tests [30,50,72]. A robust methodology for evaluating the shear modulus from results of tensile, bending and torsion tests was proposed by Pereira et al. [72].

Table 3 summarizes the numerical and analytical shear modulus results available in the literature. The only experimental result reported in the literature [8], to the best of our knowledge, was obtained by electrostatic torsion and is also shown in the Table 3. The discrepancies observed between the shear modulus values available in the literature are due to the same type of reasons above specified for the Young's modulus results: different assumptions for the value of the CNT's wall thickness, t_n, (indicated in the Table 3), modelling approaches (MD, CM, NCM), potential functions, force fields constants and formulations for shear modulus determinations. Figure 6 shows the evolutions of the shear modulus value with the nanotube diameter, D_n. In cases of Figure 6(a), the shear modulus decreases with increasing the nanotube diameter, and with further increase of the nanotube diameter, the shear modulus tends towards approximately a constant value [33,53,61,72]; in Figure 6(b) the shear modulus mainly increases with increasing the nanotube diameter [14,29,30,45,51,60,68,76,77].

Although several studies regarding the Poisson's ratio of SWCNTs have been carried out [29,30,45,52,62,72,75,77,78,80], there is still no commonly accepted value. The most common values reported in the literature are in range 0.1–0.3 (see, for example, [30,52,53,72,75,77]), but values of 0.64 [81], 0.66 [62] and close to zero [63,80] are also reported. Most authors [29,30,53,62,75,77,78,80] used the definition of Poisson's ratio for its evaluation. This requires the knowledge of the axial, $\varepsilon_{\parallel}$, and normal $\varepsilon_{\perp}$ strains in tension, as follows:

$$\nu = -\frac{\varepsilon_{\perp}}{\varepsilon_{\parallel}} \tag{15}$$

Recently, a robust methodology to assess Poisson's ratio from the results of the bending and torsion rigidities was recommended recently by Pereira et al. [65].

Figure 7 and Table 4 allow comparing the Poisson's ratio results currently available in the literature. Table 4 contains the comprehensive information on the methodology and formulation used for assessing the Poisson's ratio. Whenever possible, Table 4 also refers to whether or not it agree with the relationship $G = E\,/\,[2(1+\nu)]$, for isotropic conditions. Figure 7 and Table 4 show that the Poisson's ratio is very sensitive to different modelling approaches, analytical or numerical simulation methods, force fields constants used and formulation for Poisson's ratio assessment. For example, Dominguez-Rodriguez et al. [80] attributed the difference between the values of the Poisson's ratio obtained by the equivalent beam approach and density functional theory (DFT), to the input values of the force field constants (k_r, k_θ) in the numerical simulations. Nevertheless, the evaluation of the Poisson's ratio from the results of the tensile and torsion elastic moduli (E and G), by using the relationship $G = E\,/\,[2(1+\nu)]$, allows obtaining values similar to those determined by Eq. (15). Figure 7 also allows comparing the evolution of the Poisson's ratio value with the nanotube diameter, D_n, reported in the literature.

Table 3. Shear modulus results of SWCNTs, available in the literature.

	Reference		t_n, nm	Method	Test	Shear modulus, G, TPa	
MD	[29]	Lu, 1997	0.34	empirical force potential	tensile	0.455	av. value; non-chiral, chiral
	[30]	Jin and Yuan, 2003	0.34	force-constant approach	torsion	0.492	average value; armchair
					tensile	0.491	
				energy approach	torsion	0.547	
					tensile	0.536	
CM	[45]	Gupta and Batra, 2008	0.34	Equivalent continuum tube	torsional vibrations	0.403	av. value; non-chiral, chiral
NCM/MSM	[53]	Natsuki et al., 2004	0.34	Analytical 2D model: springs	torsion	0.300	average value; non-chiral
	[49]	Li and Chou, 2003	0.34	3D FE model: linear beams	torsion	0.480	average value; non-chiral
	[75]	Shen and Li, 2004	–	Analytical model	torsion	0.439	converged value; non-chiral
	[77]	Xiao et al., 2005	0.34	Analytical model	torsion	0.470	converged value; non-chiral
	[14]	Tserpes and Papanikos, 2005	0.147	3D FE model: linear beams	torsion	2.377	(8, 8) armchair
	[78]	Wu et al., 2006	0.268	Analytical model	torsion	0.418	converged value; non-chiral
	[60]	To, 2006	0.34	3D FE model: linear beams	torsion	0.475	(17, 0) zigzag
	[55]	Giannopoulos et al., 2008	0.34	3D FE model: linear springs	torsion	0.325	average value
	[61]	Papanikos et al., 2008	0.34	3D FE model: linear beams	torsion	0.509	converged value; non-chiral
	[51]	Cheng et al., 2010	–	Analytical model: rectangular beams	torsion	0.427	(24, 24) armchair
	[65]	Lu and Hu, 2012	0.34	3D FE model: elliptical cross section beams	torsion	0.469	(18, 18) armchair
	[68]	Giannopoulos et al., 2013	0.34	3D FE model: linear bars	torsion	0.327	converged value
	[50]	Ghavamian et al., 2013	0.34	3D FE model: linear beams	tensile	0.378	(10, 10) armchair
					torsion	0.500	
	[72]	Pereira et al., 2016	0.34	3D FE model: linear beams	tensile + bending + torsion	0.484	converged value; non-chiral, chiral
Exp	[9]	Hall et al., 2006	–	SEM	electrostatic torsion	0.410	unidentified type

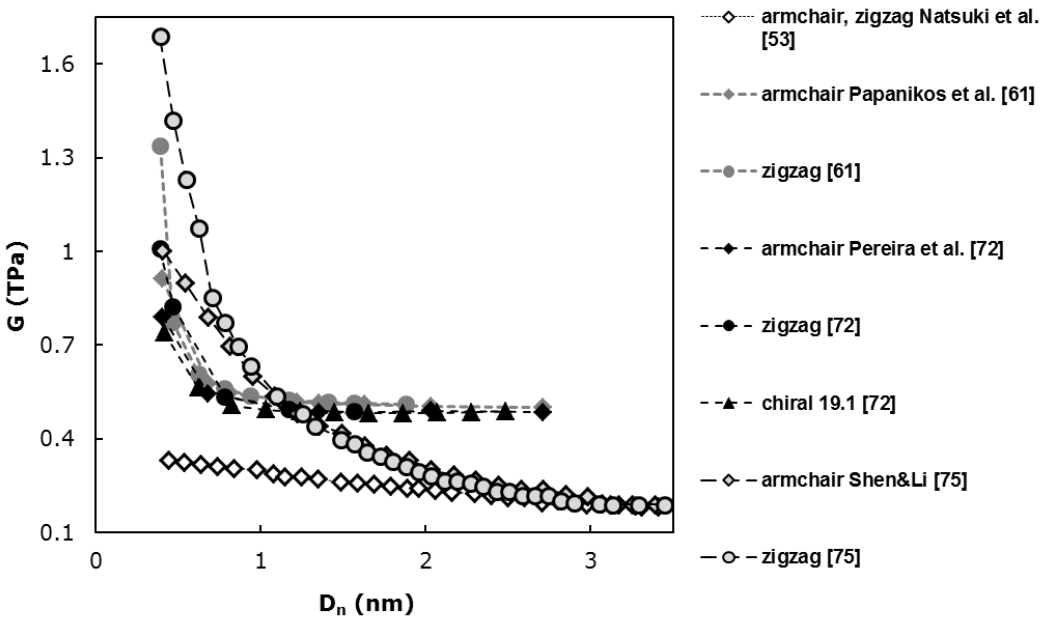

(a)

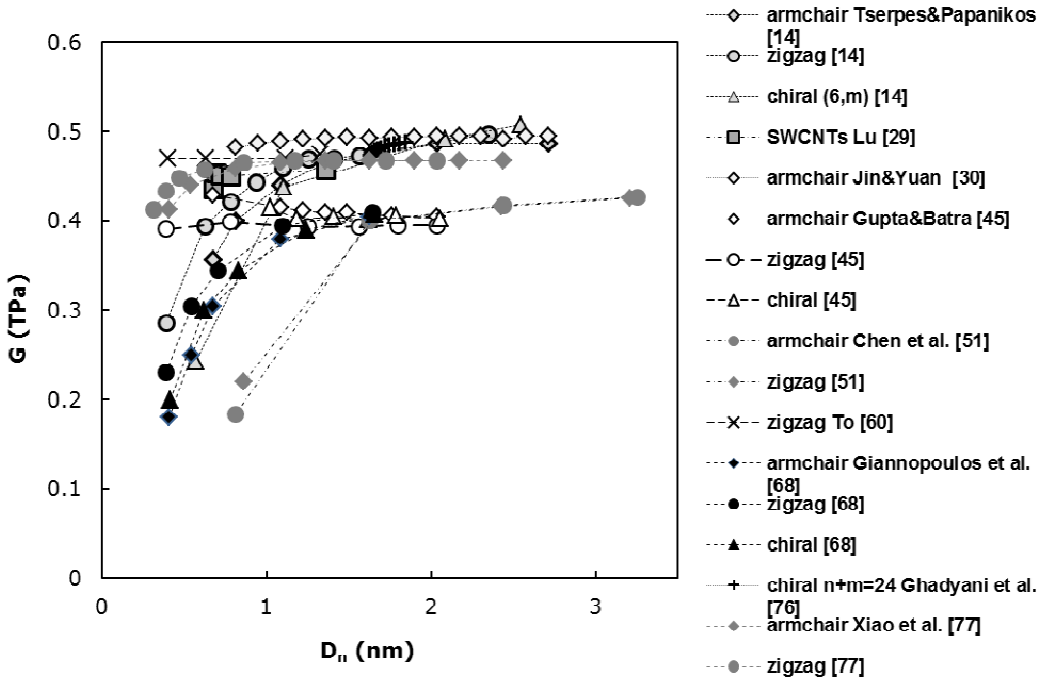

(b)

Figure 6. Literature results for the shear modulus of SWCNTs; (a) and (b) show two different trends for the evolution of the shear modulus G, with respect to the nanotube diameter, D_n.

Table 4. Poisson's ratio of SWCNTs, available in the literature.

	Reference		Method	Test	Formulation	Poisson's ratio, ν	
Atomistic approach	[27]	Lu, 1997	MD: empirical force potential	tensile	$\nu = -\varepsilon_{\perp}/\varepsilon_{\parallel}$	0.278**	average value; non-chiral, chiral
	[28]	Jin and Yuan, 2003	MD	tensile	$\nu = -\varepsilon_{\perp}/\varepsilon_{\parallel}$	0.259*	average value; armchair
	[73]	Domínguez-Rodríguez et al., 2014	*ab initio* (DFT)	tensile	$\nu = -\varepsilon_{\perp}/\varepsilon_{\parallel}$	0.185	average value; armchair
CM	[42]	Gupta and Batra, 2008	Equivalent continuum tube	axial + torsional vibrations	normal mode vibration	0.140–0.249*	non-chiral, chiral
NCM/MSM	[48]	Natsuki et al., 2004	Analytical 2D model: springs	tensile	$\nu = -\varepsilon_{\perp}/\varepsilon_{\parallel}$	0.27**	non-chiral
	[68]	Shen and Li, 2004	Analytical model	tensile	$\nu = -\varepsilon_{\perp}/\varepsilon_{\parallel}$	0.16**	converged value; non-chiral
	[70]	Xiao et al., 2005	Analytical model	tensile	$\nu = -\varepsilon_{\perp}/\varepsilon_{\parallel}$	0.2*	converged value; non-chiral
	[71]	Wu et al., 2006	Analytical model	tensile	$\nu = -\varepsilon_{\perp}/\varepsilon_{\parallel}$	0.273*	converged value; non-chiral
	[56]	Papanikos et al., 2008	3D FE model: linear beams	bending + torsion	$\nu = (\beta^*/\gamma^*) - 1$	0.056** 0.049**	armchair zigzag
	[57]	Ávila and Lacerda, 2008	3D FE model: linear beams	tensile	$\nu = -\varepsilon_{\perp}/\varepsilon_{\parallel}$	0.15–0.29	average value; non-chiral, chiral
	[73]	Domínguez-Rodríguez et al., 2014	3D FE model: linear beams	tensile	$\nu = -\varepsilon_{\perp}/\varepsilon_{\parallel}$	0.061	average value; armchair
	[52]	Eberhardt and Wallmersperger, 2015	3D FE model: tetrahedrons formed by beams	tensile	$\nu = -\varepsilon_{\perp}/\varepsilon_{\parallel}$	0.274	average value; non-chiral
	[72]	Pereira et al., 2016	3D FE model: linear beams	bending + torsion	$\nu = (EI/GJ) - 1$ $\nu = (\beta/\gamma) - 1$ (see Eqs. 10–12)	0.10*	converged value; non-chiral, chiral

β^* and γ^* relate the bending and torsion rigidities, respectively, with the chiral index, n by cubic equations: $EI = \beta^*(n - n_0)^3$ and $GJ = \gamma^*(n - n_0)^3$.

* ν value satisfies the relationship $G = E/[2(1 + \nu)]$.

** ν value does not satisfy the relationship $G = E/[2(1 + \nu)]$.

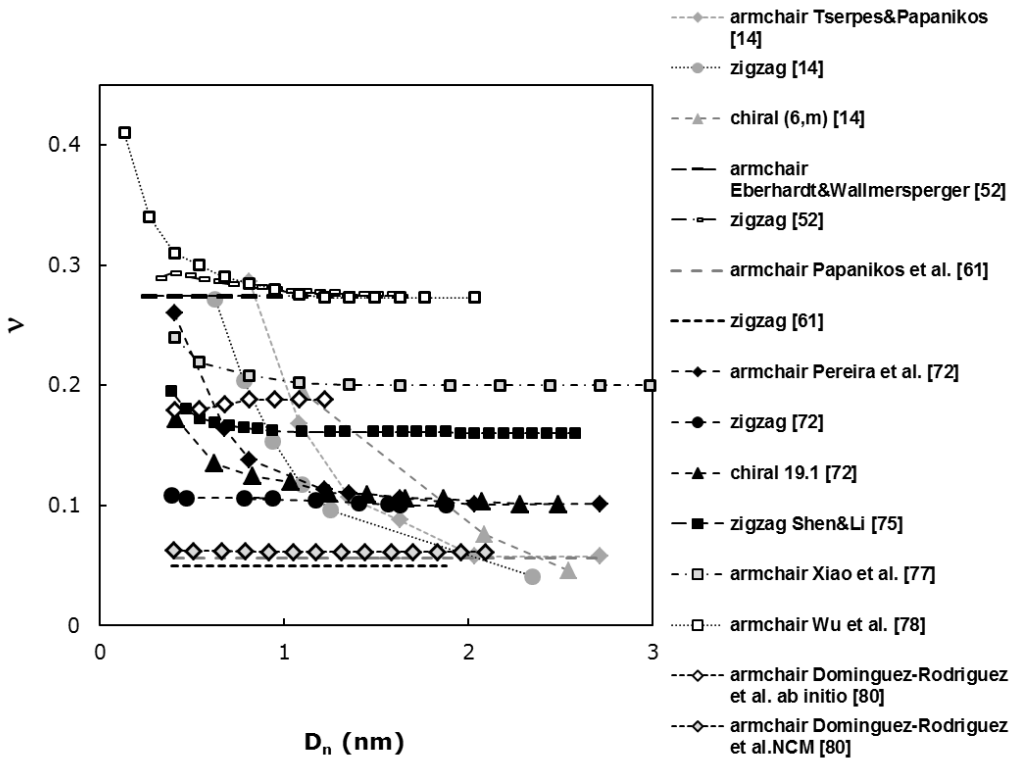

Figure 7. Literature results for the evolution of the Poisson's ratio, ν, with respect to the nanotube diameter, D_n.

4.4. Elastic Properties of SWCNTs with Vacancy Defects

The defects of the CNT's structure, such as single and multiple vacancies, show suitable effects for numerous applications of nanotubes. CNT's vacancy defects act as interfacial bonding places in reinforced nanocomposites, as storage of hydrogen and help the transition from one diameter to another in nanotube heterojunctions. The defects in CNTs are mainly due to their chemical synthesis [82] and to their chemical treatment in the purification process [83], or when the CNTs are subjected to irradiation [84].

In recent years, numerical studies regarding the effect of the defects on the CNT's mechanical properties have been carried out. For example, Scarpa et al. [85], Parvaneh and Shariati [58], Parvaneh et al. [86], Rahmandoust and Öchsner [87], Ghavamian et al. [88], Ghavamian and Öchsner [89,90], Poelma et al. [91], Sakharova et al. [92,93], Wong [94], Rafiee and Pourazizi [95], Zhang et al. [96] and Rafiee and Mahdavi [97] performed the simulations of the elastic behaviour of SWCNTs with vacancy defects; these defects consist in the absence of carbon atoms and their bonds. Other authors have reconstructed the C–C bonds near the atoms removed to form new bonds, as for example, Sharma et al. [98], Saxena and Lal [99] and Yuan and Liew [100].

The influence of vacancy defects on the Young's modulus has been extensively studied. The studies of Scarpa et al. [85], Parvaneh and Shariati [58], Parvaneh et al. [86], Rafiee and Pourazizi [95], Zhang et al. [96], Rafiee and Mahdavi [97], Sharma et al. [98], and Saxena and Lal [99] relate to a few specific types of nanotubes and vacancies, and also to relatively small

percentages of defects (less than 2.5% or in terms of the number of vacancies, up to 6).

Wong [94] considered a high number of the vacancies with several configurations, reaching a defect composed of twelve single vacancies together. Yuan and Liew [100] studied two types of vacancies (single and double ones) with percentages up to 8.0%. The studies of Sakharova et al. [92,93] have contributed to the understanding of the influence of the large amount (up to 10%) of different types of vacancies (single, double, triple and four single vacancies together) on the elastic properties of non-chiral and chiral SWCNTs, over a wide range of diameters.

The reduction of the Young's modulus observed in nanotubes with defects is a common result of the conducted studies. Several authors reported an approximately linear trend of the decreasing of Young's modulus with increasing of the number of vacancies (see, for example [87,88,92,96,97]. The literature results regarding the Young's modulus of defective SWCNTs are shown in the Table 5.

Also other SWCNTs' mechanical properties are deteriorated in presence of the vacancy defects. The studies of Ghavamian and Öchsner [89,90] showed that the presence of 0.5 and 1.0% of vacancy defects in the armchair and zigzag single-walled and multi-walled CNTs leads to a significant decrease of the CNT's critical buckling load [89] and natural frequencies [90]. Poelma et al. [91] found that the position of the single vacancy defect significantly influences the critical buckling load of the SWCNTs at low temperatures. The study of Wong [94] showed a drop of the ultimate tensile strength and the tensile failure strain when the number of vacancies increases in the armchair and zigzag SWCNTs, especially when the vacancies are situated along the cross-section of the nanotube. Saxena and Lal [99], and Sharma et al. [98] found, that the presence of vacancy defects reduces the tensile and compressive strengths, and failure strain of the nanotube. Zhang et al. [96] showed that the presence of double vacancy defect can deteriorate the radial mechanical properties of SWCNTs, reducing the collapse pressure.

For studying the fracture behaviour, some authors [12,13,101] have chosen to rebuild the C–C bonds around the atoms removed. Among their findings, a substantial reduction of the nanotube strength [13,101] and failure stresses and strains [12] should be pointed out.

5. Modelling and Elastic Properties of Multi-walled Carbon Nanotubes

In recent years, the research interest has also been focused on multi-walled carbon nanotubes (MWCNTs), i.e., structures formed by two or more concentric SWCNTs, because of their outstanding mechanical properties which can be advantageous for the improvement of structural composites and due to their high level of commercialization [102]. MWCNTs are comprised of 2 to 50 coaxial SWCNTs with an interlayer spacing generally considered similar to the interlayer spacing of graphene, 0.34 nm. The most common values experimentally determined for the interlayer distance are close to this value. For example, Kharissova and Kharisov [103] and Kiang et al. [104] reported values in the ranges of 0.32–0.35 nm and 0.342–0.375 nm, respectively. The diameter of MWCNTs can attain 30 nm in contrast to 0.7–2.0 nm for typical SWCNTs.

In spite of numerous numerical simulation studies performed towards the evaluation of the mechanical properties of carbon nanotubes, the modelling and numerical characterization of MWCNTs have received less research attention compared to SWCNTs. The essential difference between the simulation of SWCNTs and MWCNTs is to consider, in the simulation of the latter, the non-covalent weak van der Waals force. This requires significant modelling and computing efforts. The first simulations taking into account the van der Waals force were performed by Li and Chou [105],

introducing a nonlinear truss rod model in their study on the elastic behaviour of multi-walled carbon nanotubes with up to 4 layers under tension and torsion. This model comprises the complex mesh of the truss rods in addition to the beam element mesh for the simulation of each SWCNT composing the MWCNT. The studies that followed this work seek to simplify the MWCNT modelling technique. To this end, Kalmakarov et al. [41] recommended a massless non-linear spring element for the van der Waals force simulation. Also, several MWCNT's models with up to 5 layers using spring elements to describe the van der Waals interactions were successfully developed by Rahmandoust and Öchsner [79] and Ghavamian et al. [50,88]. Rahmandoust and Öchsner [79] concluded that the modelling of the van der Waals interactions between atoms of neighbour layers (SWCNTs) of the MWCNTs is not necessary in the case of uniaxial tensile test, because the MWCNT's models, whether or not taking into account the van der Waals force, showed similar Young's modulus results. In case of torsion test, a difference in the shear modulus values of about 9.0% is observed between results obtained with and without the van der Waals interactions. In their finite element model of double-walled carbon nanotubes, Fan et al. [106] proposed an interlayer pressure to model the van der Waals interaction. The mentioned models help to save the computing effort and show reasonable agreement with the results in the literature. Besides springs, other elements were tested to model the van der Waals force; for example, beam elements were used by Nahas and Abd-Rabou [107] to simulate not only the covalent C–C bonds but also the van der Waals force between layers, in double- and triple-walled CNTs. Recently, Sakharova et al. [108] have employed a simplified finite element model of MWCNTs without taking into account the van der Waals forces, but with boundary conditions allowing the simultaneous deformation of all the SWCNTs that constitute the respective MWCNT. With the help of this model, a systematic evaluation of the Young's modulus of non-chiral MWCNTs with up to 10 layers was carried out [108], from tensile and bending tests. The Young's modulus values obtained in their work [108] were in good agreement with the results available in the literature, where the van der Waals interactions were taken into account. The elastic moduli results for MWCNTs available in the literature are presented in the Table 6. In most cases, the Young's modulus and the shear modulus were calculated from the numerical results of the conventional tensile [41,50,88,105,106,107] and torsion [41,50,105,106] tests, using the respective definitions from the classical theory of elasticity. Sakharova et al. [107] evaluated the MWCNTs' Young's modulus from the values of the tensile and bending rigidities. With regard to the boundary conditions, the simulation of the MWCNT's tensile test, in the works [41,50,105,106], was achieved by subjecting all nodes at one end to the same axial force, while all nodes at the other end were fixed. In the simulation of torsion tests, Kalmakarov et al. [41] and Fan et al. [106] applied a torsional moment to all end nodes of multi-walled nanotube, when in the study of Li and Chou [105] only the outer layer of MWCNT was subjected to torsion. Ghavamian et al. [50,88], in tensile and torsion tests, Nahas and Abd-Rabou [107], in tensile tests, and Sakharova et al. [108], in tensile and bending tests, applied displacements, instead of forces or moments, to all nodes at one end of the MWCNT, leaving the other end fixed. Figure 8 compares the evolutions of the Young's modulus and shear modulus with the number of layers, N, constituting the MWCNTs.

Table 5. Results available in the literature on the reduction of the elastic moduli of SWCNTs due to vacancy defects.

Reference		Method	Numb./ percentage vac.	C–C bond reconstruction	Vac. configuration	SWCNT	E_{red} (%)	G_{red} (%)	Comments
[100]	Yuan and Liew, 2009	*ab initio* (DFT)	2.5% 8.0% 2.2% 8.5%	yes	single double	armchair (5, 5) armchair (10, 10)	≈18.0 ≈31.0 ≈21.0 ≈36.0	–	Young's modulus decreases with different rates with respect to the number of vacancy defects
[94]	Wong, 2010	MD: Tersoff–Brenner (TB) potential	8 16	no	single double 12 vac. cluster	zigzag (8, 0) armchair (10, 10)	≈12.0 ≈8.0	–	Approximately linear reduction of Young's modulus; vacancy location along the axial direction.
[58]	Parvaneh and Shariati, 2011	NCM: linear and non-linear springs	1.0% 1.25%	yes	single double triple	armchair (7, 7) zigzag (12, 0)	≈6.6 ≈8.2	–	The vacancy configuration does not influence the results.
[99]	Saxena and Lal, 2012	MD: COMPASS potential	1 4	no	single	armchair (6, 6), (10, 10)	0.9 5.09	–	Non-linear reduction of Young's modulus
[88]	Ghavamian et al., 2012	NCM: linear beams	0.5% 1.0%	no	single	armchair (10, 10) zigzag (14, 0)	≈3.8 ≈7.7	–	Linear reduction of Young's modulus: E_{red} = 7.69 Vac%.
[98]	Sharma et al., 2014	MD: COMPASS potential	1 4	yes	single	armchair (4, 4)	≈6.0 ≈17.0	≈8.0 ≈40.0	Non-linear reduction of elastic moduli.
[95]	Rafiee and Pourazizi, 2014	NCM: linear beams	1.0% 2.0%	no	single	armchair (5, 5), (7, 7) zigzag (0, 9), (0,12)	≈6.0 ≈12.0	–	Reduction of Young's modulus does not depend on the SWCNTs.
[97]	Rafiee and Mahdavi, 2016	MD: TB potential MD: REBO potential	6 6	no	single	armchair zigzag armchair zigzag	3.44 10.05 3.75 10.21	–	Approximately linear reduction of Young's modulus.
[92]	Sakharova et al., 2016	NCM: linear beams	5% 10%	no	single double triple 4 vac. cluster	non-chiral and chiral $D_n = 0.414 \div 2.713\ nm$	≈36.0 ≈43.0	≈44.0 ≈33.0	Linear reduction of both moduli up to 5% of vacancy defects: E_{red} = 7.12 Vac%; G_{red} = 8.85 Vac%.

Table 6. Results available in literature for the elastic moduli of MWCNTs, determined using NCM approaches.

	Reference	t_n, nm	Interlayer spacing, d_{int}, nm	Approach for the van der Waals interactions between layers	MWCNT	Max. number of layers	Young's modulus, TPa	Shear modulus, TPa
[105]	Li and Chou, 2003	0.34	0.339	truss rods	armchair (3, 3) (8, 8) (13, 13) (18, 18)	4	1.05–1.10	0.33–0.48
			0.352		zigzag (5, 0) (14, 0) (23, 0) (32, 0)		1.05–1.12	0.33–0.36
[41]	Kalamkarov et al., 2006	0.68	0.339	springs	armchair (5, 5) (10, 10) (15, 15) (20, 20)	4	1.00–1.45	0.44–0.47
			0.352		zigzag (5, 0) (14, 0) (23, 0) (32, 0)		0.96–1.50	0.44–0.47
[106]	Fan et al., 2009	0.34	0.352	springs: interlayer pressure	zigzag (5, 0) (14, 0) (23, 0)	3	1.006–1.011	0.43–0.34
					zigzag (18, 0) (27, 0) (36, 0)		1.040–1.019	0.36–0.33
[107]	Nahas and Abd-Rabou, 2010	0.346	–	beams	armchair	3	0.98–1.02	–
					zigzag		0.876–0.937	
[88]	Ghavamian et al., 2012	0.34	0.339	springs	armchair (10, 10) (15, 15) (20, 20) (25, 25) (30, 30)	5	1.040–1.044	–
			0.352		zigzag (14, 0) (23, 0) (32, 0) (41, 0) (50, 0)		1.030–1.035	
[50]	Ghavamian et al., 2013	0.34	0.339	springs	armchair (10, 10) (15, 15) (20, 20) (25, 25) (30, 30)	5	–	0.50
			0.352		zigzag (14, 0) (23, 0) (32, 0) (41, 0) (50, 0)			
[108]	Sakharova et al., 2017	0.34	0.339	–	armchair (10, 10) (15, 15) (20, 20) (25, 25) (30, 30) (35, 35) (40, 40) (45, 45) (50, 50) (55, 55)	10	1.061–1.054	–
			0.352		zigzag (14, 0) (23, 0) (32, 0) (41, 0) (50, 0) (59, 0) (68, 0) (77, 0) (86, 0) (95, 0)		1.069–1.012	

Some authors [105,106,107] pointed out that Young's modulus of MWCNTs is slightly higher than that of SWCNTs. The Young's modulus values for MWCNTs, which are very close to the values obtained for SWCNTs constituting the MWCNT, were also reported [88,108]. A substantial increase of the Young's modulus with the number of layers was reported by Kalmakarov et al. [41]. Shear modulus trends similar to the trend for the Young's modulus of MWCNTs were described in the works of Kalmakarov et al. [41] and Ghavamian et al. [50]. Li and Chou [105] and Fan et al. [106] reported values of the MWCNTs' shear modulus slightly lower than those of SWCNTs.

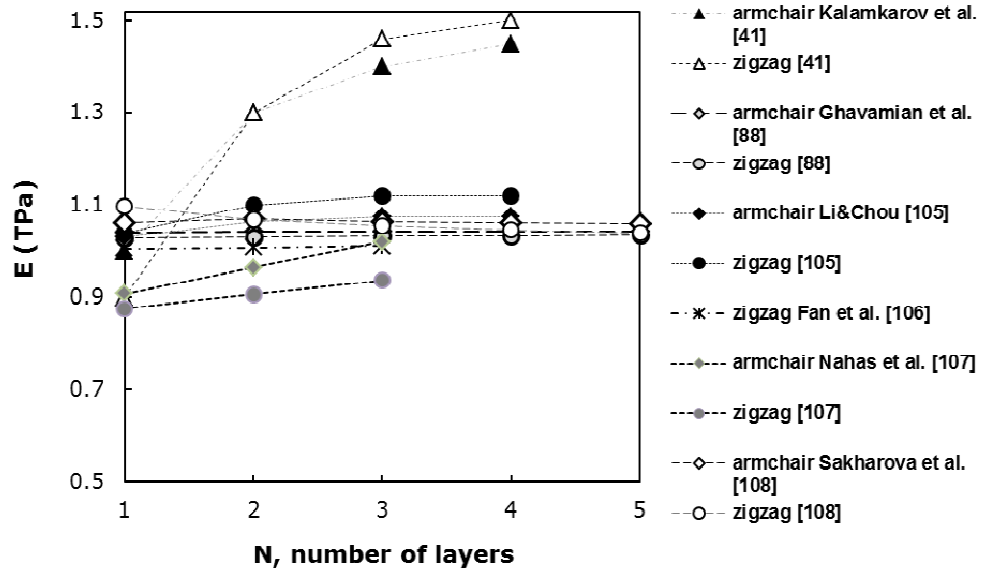

(a)

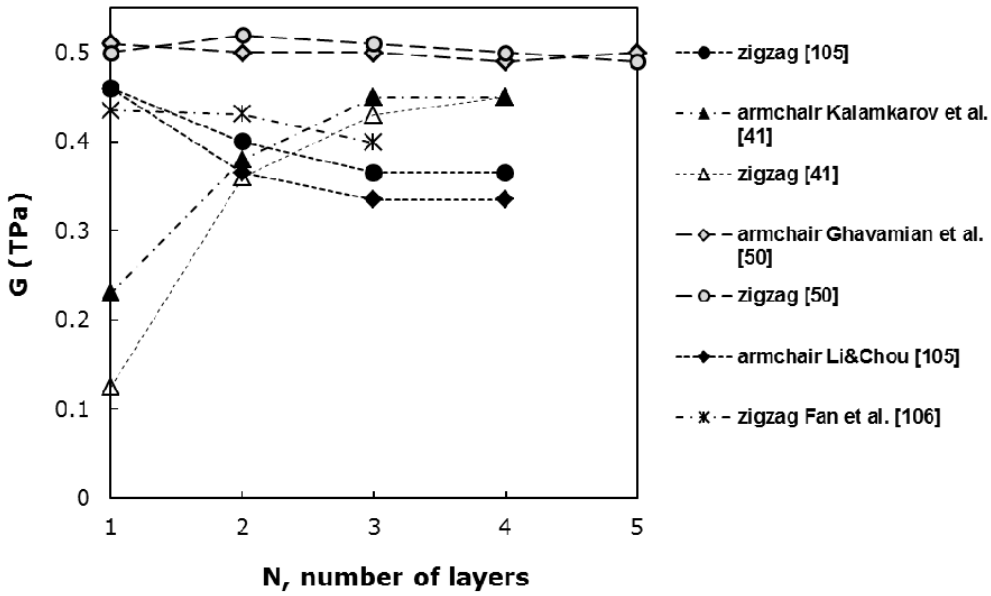

(b)

Figure 8. Literature results for elastic moduli of MWCNTs: (a) Young's modulus and (b) shear modulus with respect to the number of layers, N, constituting the MWCNT.

6. Modelling and Mechanical Behaviour of CNT HJs

From the point of view of the construction of nanodevices, the CNT junctions are necessary constituents for circuits, amplifiers, switches, rectifiers, molecular storages, field-effect transistors and nanodiodes. A comprehensive review on synthesis, properties and realistic applications of CNT junctions was published by Wei and Liu [6]. CNT HJs have attracted special research interest, because of their singular electrical and optical properties, and potentially attractive applications as nanodiodes and filters [109,110]. Despite the progress achieved in recent years in this research field, many challenges still remain. One of them is to understand the deformation behaviour of CNT heterojunctions, since the stability and efficiency of the nanodevices is highly dependent on the mechanical properties of their components.

Molecular dynamics and nanoscale continuum approaches combined with finite element modelling have become the most prevalent methods to simulate the mechanical behaviour of CNT heterojunctions. A few studies were performed using the MD approach [24,26,111]. Lee and Su [111] investigated the temperature effect on the mechanical properties, yield stress and Young's modulus, of (6, 0)–(8, 0) SWCNT HJs under tension and compression, by using an MD simulation approach, employing a REBO potential to describe the carbon–carbon (C–C) interaction. Also employing a REBO potential, Li et al. [24] investigated the tensile strength and failure modes of single-walled and double-walled CNT HJs at different temperatures and strain rates.

Qin et al. [26] performed an MD simulation study, using second-generation Tersoff–Brenner potential, in order to evaluate Young's modulus and failure stress of single-walled and double-walled CNT HJs. Kang et al. [112], also using MD simulation with Tersoff–Brenner potential coupled with NCM approach, studied the buckling behaviour of (7, 7)–(9, 9) HJs under compression. Kinoshita et al. [113] used *ab initio* density functional theory calculations in order to assess the Young's modulus and stress–strain relationship for (8, 0)–(6, 0)–(8, 0) SWCNT HJs structures. An MD simulation, employing second-generation Tersoff–Brenner potential, was used by Xi et al. [114] in order to study the mechanical behaviour of complex HJs structures consisting of four (n, n) armchair and five $(2n, 0)$ zigzag SWCNTs.

The studies using the NCM approach were devoted to the characterization of the buckling [115,116], tensile [22,25,116,117,118,119] and shear [22,25,116,120] behaviour of HJs, and the evaluation of their Poisson's ratio [110]. Sakharova et al. [22], analysing the mechanical behaviour of the armchair–armchair and zigzag–zigzag HJs, pointed out the occurrence of redundant bending deformation during the tensile test, making it difficult to analyse this test. Scarpa et al. [110] also reported this aspect when calculating the Poisson's ratio from the tensile test of (5, 5)–(10, 10) HJs.

Regarding the evaluation of the HJs elastic properties such as rigidities, Young's and shear moduli, some of the authors reported their decrease when compared with the elastic properties of the constituent SWCNTs [22,25,116,117,119]. The literature results on the studies of the heterojunction elastic properties are resumed in Table 7. The aforementioned investigations must be understood as the beginning of broader necessary studies on the mechanical properties of the carbon nanotube heterojunctions.

Table 7. Results for the elastic moduli of CNT HJs available in literature.

	Reference	Method	Type of HJs	*Young's modulus, E, TPa	*Shear modulus, G, TPa	Comments
[26]	Qin et al., 2008	MD: Tersoff-Brenner potential	armchair–armchair (5, 5)–(7, 7), (5, 5)–(8, 8), …(5, 5)–(10, 10)	0.775	–	Young's modulus of HJ about 20% higher than for the narrower (5, 5) or (9, 0) SWCNT;
			zigzag–zigzag (9, 0)–(10, 0), (9, 0)–(11, 0), …(9, 0)–(14, 0)	0.795	–	E value increases with increasing the HJ average diameter.
			double-walled, triple-walled and four-walled armchair composed by (5, 5), (10, 10), (15, 15), ...(25, 25)	0.773	–	Young's modulus decreases with the number of SWCNTs constituting an N-walled CNT heterojunction.
[110]	Scarpa et al., 2011	NCM: linear beams	armchair–armchair (5, 5)–(10, 10)	1.010	–	Bending deformation of HJ in tension were taken into account.
			zigzag–zigzag (9, 0)–(14, 0)	0.945		
[113]	Kinoshita et al., 2013	*ab initio* (DFT) with AIREBO potential	zigzag–zigzag–zigzag (8, 0)–(6, 0)–(8, 0)	0.995	–	The Young's modulus for a HJ structure is lower at about 10.23% than for the narrower (6, 0) SWCNT and at about 4.25% than for the wider (8, 0) SWCNT.
[117]	Hemmatian et al., 2014	NCM: linear beams	armchair–armchair (5, 5)–(10, 10), (10, 10)–(15, 15), …(25, 25)–(30, 30)	1.109	0.344	Elastic moduli are lower than those for constituent SWCNTs; E and G increase with increasing the HJ average diameter, $\overline{D}_{HJ}$, and decrease with increasing of overall length L_{HJ}.
[116]	Ghavamian and Ochsner, 2015;	NCM: linear beams	armchair–armchair composed by a variety of SWCNTs in a range of (3, 3) to (18, 18)	0.927	0.180	Elastic moduli are lower than those for constituent SWCNTs.
[119]	Yengejeh et al., 2015		zigzag–zigzag composed by a variety of SWCNTs in a range of (6, 0) to (19, 0)	0.939	0.270	
[22]	Ghavamian et al., 2015;	NCM: linear beams	armchair–zigzag with bent connection	0.177	0.179	The Young's modulus of HJs decreases drastically; the shear modulus is close to that of the constituent SWCNTs.
[116]	Ghavamian and Ochsner, 2015		chiral–armchair (zigzag) with bent connection	0.160	0.220	
[25]	Sakharova et al., 2016	NCM: linear beams	armchair–armchair (5, 5)–(10, 10), (10, 10)–(15, 15), (15, 15)–(20, 20)	Bending (EI) and torsional (GJ) rigidities increase with increasing the HJ average diameter. EI rigidities are comparable with those for narrower SWCNTs. GJ rigidities are higher than for narrower SWCNTs, and lower than for wider SWCNTs.		
			zigzag–zigzag (5, 0)–(10, 0), (10, 0)–(15, 0), (15, 0)–(20, 0)			

* Average values.

7. Conclusions

This review shows that a great investment has been made lately in the development of the modelling of mechanical properties of carbon nanotubes. These include the elastic moduli and the Poisson ratio of single and multi-walled carbon nanotubes and their heterojunctions, without and with vacancy defects. In spite of great developments has been made in predicting the mechanical properties of CNTs by numerical simulation, the theoretical studies (analytical and numerical) have led to some variety of results due to different modelling approaches and formulations. The resulting scattering in the values of the elastic constants raises questions on the reliability of the data obtained and can affect its interpretation. Among the several approaches, the nanoscale continuum modelling (NCM/MSM) proves to be efficient for simulating the nanotubes behaviour without requiring extensive computation.

Acknowledgments

The authors gratefully acknowledge the financial support of the Portuguese Foundation for Science and Technology (FCT), Portugal, via Projects PTDC/EMS-TEC/0702/2014 (POCI-01-0145-FEDER-016779), PTDC/EMS-TEC/6400/2014 (POCI-01-0145-FEDER-016876), and UID/EMS/00285/2013, by UE/FEDER through Program COMPETE2020. N. A. Sakharova and A. F. G. Pereira were supported by a grant for scientific research from the Portuguese Foundation for Science and Technology (refs. SFRH/BPD/107888/2015, and SFRH/BD/102519/2014, resp.). All supports are gratefully acknowledged.

Conflict of Interest

The authors declare that there is no conflict of interest regarding the publication of this manuscript.

References

1. Robertson J (2004) Realistic applications of CNTs. *Mater Today* 7: 46–52.
2. Dresselhaus MS, Avouris P (2001) Introduction to carbon materials research, In: Dresselhaus, MS, Dresselhaus G, Avouris P, *Carbon Nanotubes: Synthesis, Structure, Properties, and Applications*, Springer Book Series: Topics in Applied Physics, Germany: Springer-Verlag Berlin Heidelberg, 80: 1–9.
3. Neubauer E, Kitzmantel M, Hulman M, et al. (2010) Potential and challenges of metal-matrix-composites reinforced with carbon nanofibers and carbon nanotubes. *Compos Sci Technol* 70: 2228–2236.
4. Lan Y, Wang Y, Ren ZF (2011) Physics and applications of aligned carbon nanotubes. *Adv Phys* 60: 553–678.
5. Zhang Y, Zhuang X, Muthu J, et al. (2014) Load transfer of graphene/carbon nanotube/polyethylene hybrid nanocomposite by molecular dynamics simulation. *Compos Part B-Eng* 63: 27–33.

6. Schulz MJ, Shanov VN, Yin Z (2014) *Nanotube superfiber Materials*, Oxford (UK): Elsevier, 848.
7. Wei DC, Liu YQ (2008) The intramolecular junctions of carbon nanotubes. *Adv Mater* 20: 2815–2841.
8. Salvetat JP, Briggs GAD, Bonard JM, et al. (1999) Elastic and shear moduli of single-walled carbon nanotube ropes. *Phys Rev Lett* 82: 944–947.
9. Hall AR, An L, Liu J, et al. (2006) Experimental measurement of single-wall carbon nanotube torsional properties. *Phys Rev Lett* 96: 256102.
10. Kallesøe C, Larsen MB, Bøggild P, et al. (2012) 3D mechanical measurements with an atomic force microscope on 1D structures. *Rev Sci Instrum* 83: 023704.
11. Wang L, Zhang Z, Han X (2013) In situ experimental mechanics of nanomaterials at the atomic scale. *NPG Asia Mater* 5: e40.
12. Mielke SL, Troya D, Zhan S, et al. (2004) The role of vacancy defects and holes in the fracture of carbon nanotubes. *Chem Phys Lett* 390: 413–420.
13. Hou W, Xiao S (2007) Mechanical behaviors of carbon nanotubes with randomly located vacancy defects. *J Nanosci Nanotechnol* 7: 4478–4485.
14. Tserpes KI, Papanikos P (2005) Finite element modeling of single-walled carbon nanotubes. *Compos Part B-Eng* 36: 468–477.
15. Rafiee R, Heidarhaei M (2012) Investigation of chirality and diameter effects on the Young's modulus of carbon nanotubes using non-linear potentials. *Compos Struct* 94: 2460–2464.
16. Sakharova NA, Pereira AFG, Antunes JM, et al. (2015) Mechanical characterization of single-walled carbon nanotubes: Numerical simulation study. *Compos Part B-Eng* 75: 73–85.
17. Rafiee R, Moghadam RM (2014) On the modelling of carbon nanotubes: A critical review. *Compos Part B-Eng* 56: 435–449.
18. Yengejeh SI, Kazemi SA, Öchsner A (2016) Advances in mechanical analysis of structurally and atomically modified carbon nanotubes and degenerated nanostructures: A review. *Compos Part B-Eng* 86: 95–107.
19. Dresselhaus MS, Dresselhaus G, Saito R (1995) Physics of carbon nanotubes. *Carbon* 33: 883–891.
20. Barros EB, Jorio A, Samsonidze GG, et al. (2006) Review on the symmetry-related properties of carbon nanotubes. *Phys Rep* 431: 261–302.
21. Melchor S, Dobado JA (2004) CoNTub: An algorithm for connecting two arbitrary carbon nanotubes. *J Chem Inf Comp Sci* 44: 1639–1646.
22. Ghavamian A, Andriyana A, Chin AB, et al. (2015) Numerical investigation on the influence of atomic defects on the tensile and torsional behavior of hetero-junction carbon nanotubes. *Mater Chem Phys* 164: 122–137.
23. Yao YG, Li QW, Zhang J, et al. (2007) Temperature-mediated growth of single-walled carbon-nanotube intramolecular junctions. *Nat Mater* 6: 283–286.
24. Li M, Kang Z, Li R, et al. (2013) A molecular dynamics study on tensile strength and failure modes of carbon nanotube junctions. *J Phys D Appl Phys* 46: 495301.
25. Sakharova NA, Pereira AFG, Antunes JM, et al. (2016) Numerical simulation of the mechanical behaviour of single-walled carbon nanotubes heterojunctions. *J Nano Res* 38: 73–87.
26. Qin Z, Qin QH, Feng XQ (2008) Mechanical property of carbon nanotubes with intramolecular junctions: Molecular dynamics simulations. *Phys Lett A* 372: 6661–6666.

27. Lu Q, Bhattacharya B (2005) The role of atomistic simulations in probing the small scale aspects of fracture—a case study on a single-walled carbon nanotube. *Eng Fract Mech* 72: 2037–2071.
28. Yakobson BI, Brabec CJ, Bernholc J (1996) Nanomechanics of carbon tubes: instabilities beyond linear response. *Phys Rev Lett* 76: 2511–2514.
29. Lu JP (1997) Elastic properties of carbon nanotubes and nanoropes. *Phys Rev Lett* 79: 1298–1300.
30. Jin Y, Yuan FG (2003) Simulation of elastic properties of single-walled carbon nanotubes. *Compos Sci Technol* 63: 1507–1515.
31. Liew KM, He XQ, Wong CH (2004) On the study of elastic and plastic properties of multi-walled carbon nanotubes under axial tension using molecular dynamics simulation. *Acta Mater* 52: 2521–2527.
32. Bao WX, Zhu CC, Cui WZ (2004) Simulation of Young's modulus of single-walled carbon nanotubes by molecular dynamics. *Physica B* 352: 156–163.
33. Zhang HW, Wang JB, Guo X (2005) Predicting the elastic properties of single-walled carbon nanotubes. *J Mech Phys Solids* 53: 1929–1950.
34. Cheng HC, Liu YL, Hsu YC, et al. (2009) Atomistic continuum modelling for mechanical properties of single-walled carbon nanotubes. *Int J Solids Struct* 46: 1695–1704.
35. Kudin KN, Scuseria GE, Yakobson BI (2001) C_2F, BN and C nanoshell elasticity from ab initio computations. *Phys Rev B* 64: 235406.
36. Wilmes AA, Pinho ST (2014) A coupled mechanical-charge/dipole molecular dynamics finite element method, with multi-scale applications to the design of graphene nano-devices. *Int J Numer Meth Eng* 100: 243–276.
37. Hernandez E, Goze C, Bernier P, et al. (1998) Elastic properties of C and $B_xC_yN_z$ composite nanotubes. *Phys Rev Lett* 80: 4502–4505.
38. Zhou X, Zhou J, Ou-Yang ZC (2000) Strain energy and Young's modulus of single-wall carbon nanotubes calculated from electronic energy-band theory. *Phys Rev B* 62: 13692–13696.
39. Ru CQ (2000) Effective bending stiffness of carbon nanotubes. *Phys Rev B* 62: 9973–9976.
40. Pantano A, Parks DM, Boyce MC (2004) Mechanics of deformation of single- and multi-wall carbon nanotubes. *J Mech Phys Solids* 52: 789–821.
41. Kalamkarov AL, Georgiades AV, Rokkam SK, et al. (2006) Analytical and numerical techniques to predict carbon nanotubes properties. *Int J Solids Struct* 43: 6832–6854.
42. Muc A (2010) Design and identification methods of effective mechanical properties for carbon nanotubes. *Mater Design* 31: 1671–1675.
43. Chang TC (2010) A molecular based anisotropic shell model for single-walled carbon nanotubes. *J Mech Phys Solids* 58: 1422–1433.
44. Sears A, Batra RC (2004) Macroscopic properties of carbon nanotubes from molecular-mechanics simulations. *Phys Rev B* 69: 235406.
45. Gupta SS, Batra RC (2008) Continuum structures equivalent in normal mode vibrations to single-walled carbon nanotubes. *Comp Mater Sci* 43: 715–723.
46. Wang Q (2004) Effective in-plane stiffness and bending rigidity of armchair and zigzag carbon nanotubes. *Int J Solids Struct* 41: 5451–5461.
47. Arash B, Wang Q (2012) A review on the application of nonlocal elastic models in modelling of carbon nanotubes and graphenes. *Comp Mater Sci* 51: 303–313.

48. Odegard GM, Gates TS, Nicholson LM, et al. (2002) Equivalent continuum modelling of nano-structured materials. *Compos Sci Technol* 62: 1869–1880.
49. Li C, Chou TW (2003) A structural mechanics approach for the analysis of carbon nanotubes. *Int J Solids Struct* 40: 2487–2499.
50. Ghavamian A, Rahmandoust M, Öchsner A (2013) On the determination of the shear modulus of carbon nanotubes. *Compos Part B-Eng* 44: 52–59.
51. Chen WH, Cheng HC, Liu YL (2010) Radial mechanical properties of single-walled carbon nanotubes using modified molecular structure mechanics. *Comp Mater Sci* 47: 985–993.
52. Eberhardt O, Wallmersperger T (2015) Energy consistent modified molecular structural mechanics model for the determination of the elastic properties of single wall carbon nanotubes. *Carbon* 95: 166–180.
53. Natsuki T, Tantrakarn K, Endo M (2004) Prediction of elastic properties for single-walled carbon nanotubes. *Carbon* 42: 39–45.
54. Meo M, Rossi M (2006) Prediction of Young's modulus of single wall carbon nanotubes by molecular-mechanics based finite element modeling. *Compos Sci Technol* 66: 1597–1605.
55. Giannopoulos GI, Kakavas PA, Anifantis NK (2008) Evaluation of the effective mechanical properties of single-walled carbon nanotubes using a spring based finite element approach. *Comp Mater Sci* 41: 561–569.
56. Wernik JM, Meguid SA (2010) Atomistic-based continuum modelling of the nonlinear behavior of carbon nanotubes. *Acta Mech* 212: 167–179.
57. Ranjbartoreh AZ, Wang G (2010) Consideration of mechanical properties of single-walled carbon nanotubes under various loading conditions. *J Nanopart Res* 12: 537–543.
58. Parvaneh V, Shariati M (2011) Effect of defects and loading on prediction of Young's modulus of SWCNTs. *Acta Mech* 216: 281–289.
59. Mahmoudinezhad E, Ansari R, Basti A, et al. (2012) An accurate spring-mass model for predicting mechanical properties of single-walled carbon nanotubes. *Comp Mater Sci* 62: 6–11.
60. To CWS (2006) Bending and shear moduli of single-walled carbon nanotubes. *Finite Elem Anal Design* 42: 404–413.
61. Papanikos P, Nikolopoulos DD, Tserpes KI (2008) Equivalent beams for carbon nanotubes. *Comp Mater Sci* 43: 345–352.
62. Ávila AF, Lacerda GSR (2008) Molecular mechanics applied to single-walled carbon nanotubes. *Mater Res* 11: 325–333.
63. Shokrieh MM, Rafiee R (2010) Prediction of Young's modulus of graphene sheets and carbon nanotubes using nanoscale continuum mechanics approach. *Mater Design* 31: 790–795.
64. Her SC, Liu SJ (2012) Theoretical prediction of tensile behavior of single-walled carbon nanotubes. *Curr Nanosci* 8: 42–46.
65. Lu X, Hu Z (2012) Mechanical property evaluation of single-walled carbon nanotubes by finite element modeling. *Compos Part B-Eng* 43: 1902–1913.
66. Mohammadpour E, Awang M (2011) Predicting the nonlinear tensile behavior of carbon nanotubes using finite element simulation. *Appl Phys A-Mater* 104: 609–614.
67. Ghadyani G, Öchsner A (2015) Derivation of a universal estimate for the stiffness of carbon nanotubes. *Physica E* 73: 116–125.

68. Giannopoulos GI, Tsiros AP, Georgantzinos SK (2013) Prediction of Elastic Mechanical Behavior and Stability of Single-Walled Carbon Nanotubes Using Bar Elements. *Mech Adv Mater Struct* 20: 730–741.
69. Nasdala L, Ernst G (2005) Development of a 4-node finite element for the computation of nano-structured materials. *Comp Mater Sci* 33: 443–458.
70. Budyka MF, Zyubina TS, Ryabenko AG, et al. (2005) Bond lengths and diameters of armchair single wall carbon nanotubes. *Chem Phys Lett* 407: 266–271.
71. Ghadyani G, Öchsner A (2015) On a thickness free expression for the stiffness of carbon nanotubes. *Solid State Commun* 209: 38–44.
72. Pereira AFG, Antunes JM, Fernandes JV, et al. (2016) Shear modulus and Poisson's ratio of single-walled carbon nanotubes: numerical evaluation. *Phys Status Solidi B* 253: 366–376.
73. Krishnan A, Dujardin E, Ebbesen TW, et al. (1998) Young's modulus of single-walled nanotubes. *Phys Rev B* 58: 14013–14018.
74. Yu MF, Files BS, Arepalli S, et al. (2000) Tensile loading of ropes of single wall carbon nanotubes and their mechanical properties. *Phys Rev Lett* 84: 5552–5554.
75. Shen L, Li J (2004) Transversely isotropic elastic properties of single-walled carbon nanotubes. *Phys Rev B* 69: 045414.
76. Ghadyani G, Soufeiani L, Öchsner A (2017) Angle dependence of the shear behaviour of asymmetric carbon nanotubes. *Mater Design* 116:136–143.
77. Xiao JR, Gama BA, Gillespie Jr JW (2005) An analytical molecular structural mechanics model for the mechanical properties of carbon nanotubes. *Int J Solids Struct* 42: 3075–3092.
78. Wu Y, Zhang X, Leung AYT, et al. (2006) An energy-equivalent model on studying the mechanical properties of single-walled carbon nanotubes. *Thin Wall Struct* 44: 667–676.
79. Rahmandoust M, Öchsner A (2012) On finite element modeling of single- and multi-walled carbon nanotubes. *J Nanosci Nanotechnol* 12: 8129–8136.
80. Domínguez-Rodríguez G, Tapia A, Avilés F (2014) An assessment of finite element analysis to predict the elastic modulus and Poisson's ratio of singlewall carbon nanotubes. *Comp Mater Sci* 82: 257–263.
81. Popov VN, Van Doren VE, Balkanski M (2000) Elastic Properties of single-walled carbon nanotubes. *Phys Rev B* 61: 3078–3084.
82. Gao RP, Wang ZL, Bai ZG, et al. (2000) Nanomechanics of individual carbon nanotubes from pyrolytically grown arrays. *Phys Rev Lett* 85: 622–625.
83. Andrews R, Jacques D, Qian D, et al. (2001) Purification and structural annealing of multiwalled carbon nanotubes at graphitization temperatures. *Carbon* 39: 1681–1687.
84. Terrones M, Banhart F, Grobert N, et al. (2002) Molecular junctions by joining single-walled carbon nanotubes. *Phys Rev Lett* 89: 075505.
85. Scarpa F, Adhikari S, Wang CY (2009) Mechanical properties of non-reconstructed defective single-wall carbon nanotubes. *J Phys D Appl Phys* 42: 142002.
86. Parvaneh V, Shariati M, Torabi H (2012) Bending buckling behavior of perfect and defective single-walled carbon nanotubes via a structural mechanics model. *Acta Mech* 223: 2369–2378.
87. Rahmandoust M, Öchsner A (2009) Influence of structural imperfections and doping on the mechanical properties of single-walled carbon nanotubes. *J Nano Res* 6: 185–196.

88. Ghavamian A, Rahmandoust M, Öchsner A (2012) A numerical evaluation of the influence of defects on the elastic modulus of single and multi-walled carbon nanotubes. *Comp Mater Sci* 62: 110–116.
89. Ghavamian A, Öchsner A (2012) Numerical investigation on the influence of defects on the buckling behavior of single-and multi-walled carbon nanotubes. *Physica E* 46: 241–249.
90. Ghavamian A, Öchsner A (2013) Numerical modeling of eigenmodes and eigenfrequencies of single- and multi-walled carbon nanotubes under the influence of atomic defects. *Comp Mater Sci* 72: 42–48.
91. Poelma RH, Sadeghian H, Koh S, et al. (2012) Effects of single vacancy defect position on the stability of carbon nanotubes. *Microelectron Reliab* 52: 1279–1284.
92. Sakharova NA, Pereira AFG, Antunes JM, et al. (2016) Numerical simulation study of the elastic properties of single-walled carbon nanotubes containing vacancy defects. *Compos Part B-Eng* 89: 155–168.
93. Sakharova NA, Antunes JM, Pereira AFG, et al. (2015) The effect of vacancy defects on the evaluation of the mechanical properties of single-wall carbon nanotubes: Numerical simulation study, In: Öchsner A, Altenbach H, *Springer Book Series On Advanced Structured Materials: Mechanical and Materials Engineering of Modern Structure and Component Design*, Germany: Springer, 70: 323–339.
94. Wong CH (2010) Elastic properties of imperfect single-walled carbon nanotubes under axial tension. *Comp Mater Sci* 49: 143–147.
95. Rafiee R, Pourazizi R (2014) Evaluating the Influence of Defects on the Young's Modulus of Carbon Nanotubes Using Stochastic Modeling. *Mater Res* 17: 758–766.
96. Zhang YP, Ling CC, Li GX, et al. (2015) Radial collapse and physical mechanism of carbon nanotube with divacancy and 5-8-5 defects. *Chinese Phys B* 24: 046401.
97. Rafiee R, Mahdavi M (2016) Molecular dynamics simulation of defected carbon nanotubes. *P I Mech Eng L-J Mat* 230: 654–662.
98. Sharma S, Chandra R, Kumar P, et al. (2014) Effect of Stone-Wales and vacancy defects on elastic moduli of carbon nanotubes and their composites using molecular dynamics simulation. *Comp Mater Sci* 86: 1–8.
99. Saxena KK, Lal A (2012) Comparative molecular dynamics simulation study of mechanical properties of carbon nanotubes with number of Stone-Wales and vacancy defects. *Procedia Eng* 38: 2347–2355.
100. Yuan J, Liew KM (2009) Effects of vacancy defect reconstruction on the elastic properties of carbon nanotubes. *Carbon* 47: 1526–1533.
101. Xiao S, Hou W (2006) Fracture of vacancy-defected carbon nanotubes and their embedded nanocomposites. *Phys Rev B* 73: 115406.
102. Kurita H, Estili M, Kwon H, et al. (2015) Load-bearing contribution of multi-walled carbon nanotubes on tensile response of aluminium. *Compos Part A-Appl S* 68: 133–139.
103. Kharissova OV, Kharisov BI (2014) Variations of interlayer spacing in carbon nanotubes. *RSC Adv* 58: 30807–30815.
104. Kiang CH, Endo M, Ajayan PM, et al. (1998) Size effects in carbon nanotubes. *Phys Rev Lett* 81: 1869–1872.
105. Li C, Chou TW (2003) Elastic moduli of multi-walled carbon nanotubes and the effect of van der Waals forces. *Comp Sci Tech* 63: 1517–1524.

106. Fan CW, Liu YY, Hwu C (2009) Finite element simulation for estimating the mechanical properties of multi-walled carbon nanotubes. *Appl Phys A-Mater* 5: 819–831.
107. Nahas MN, Abd-Rabou M (2010) Finite element modeling of multi-walled carbon nanotubes. *Int J Eng Technol* 10: 63–71.
108. Sakharova NA, Pereira AFG, Antunes JM, et al. (2017) Numerical simulation on the mechanical behaviour of the multi-walled carbon nanotubes. *J Nano Res* 47: 106–119.
109. Liu Q, Liu W, Cui ZM, et al. (2007) Synthesis and characterization of 3D double branched K junction carbon nanotubes and nanorods. *Carbon* 45: 268–273.
110. Scarpa F, Narojczyk JW, Wojciechowski KW (2011) Unusual deformation mechanisms in carbon nanotube heterojunctions (5, 5)–(10, 10) under tensile loading. *Phys Status Solidi B* 248: 82–87.
111. Lee WJ, Su WS (2013) Investigation into the mechanical properties of single-walled carbon nanotube heterojunctions. *Phys Chem Chem Phys* 15: 11579–11585.
112. Kang Z, Li M, Tang Q (2010) Buckling behavior of carbon nanotube-based intramolecular junctions under compression: Molecular dynamics simulation and finite element analysis. *Comp Mater Sci* 50: 253–259.
113. Kinoshita Y, Murashima M, Kawachi M, et al. (2013) First-principles study of mechanical properties of one-dimensional carbon nanotube intramolecular junctions. *Comp Mater Sci* 70: 1–7.
114. Xi H, Song HY, Zou R (2015) Simulation of mechanical properties of carbon nanotubes with superlattice structure. *Curr Appl Phys* 15: 1216–1221.
115. Yengejeh SI, Zadeh MA, Öchsner A (2014) On the buckling behavior of connected carbon nanotubes with parallel longitudinal axes. *Appl Phys A-Mater* 115: 1335–1344.
116. Ghavamian A, Öchsner A (2015) A comprehensive numerical investigation on the mechanical properties of hetero-junction carbon nanotubes. *Commun Theor Phys* 64: 215–230.
117. Hemmatian H, Fereidoon A, Rajabpour M (2014) Mechanical properties investigation of defected, twisted, elliptic, bended and hetero-junction carbon nanotubes based on FEM. *Fuller Nanotub Car N* 22: 528–544.
118. Rajabpour M, Hemmatian H, Fereidoon A (2011) Investigation of Length and Chirality Effects on Young's Modulus of Heterojunction Nanotube with FEM. Proceedings of the 2nd International Conference on Nanotechnology: Fundamentals and Applications, Ottawa, Ontario, Canada.
119. Yengejeh SI, Zadeh MA, Öchsner A (2015) On the tensile behavior of hetero-junction carbon nanotubes. *Compos Part B-Eng* 75: 274–280.
120. Yengejeh SI, Zadeh MA, Öchsner A (2014) Numerical characterization of the shear behavior of hetero-junction carbon nanotubes. *J Nano Res* 26: 143–151.

AIMS Press